Proceedings of the ASME 2021
Fluids Engineering Division Summer Meeting
FEDSM2021
August 10-12, 2021, Virtual, Online

FEDSM2021-65792

COMPUTATIONAL INVESTIGATION OF THRUST PRODUCTION OF A DOLPHIN AT VARIOUS SWIMMING SPEEDS

Junshi Wang
Department of Mechanical and Aerospace Engineering,
University of Virginia
Charlottesville, VA, USA

Vadim Pavlov
Department of Biology,
Hopkins Marine Station
Stanford University
Pacific Grove, CA, USA

Zhipeng Lou
Department of Mechanical and Aerospace Engineering,
University of Virginia
Charlottesville, VA, USA

Haibo Dong[1]
Department of Mechanical and Aerospace Engineering
University of Virginia
Charlottesville, VA, USA

ABSTRACT

Dolphins are known for their outstanding swimming performance. However, the difference in flow physics at different speeds remains elusive. In this work, the underlying mechanisms of dolphin swimming at three speeds, 2 m/s, 5 m/s, and 8 m/s, are explored using a combined experimental and numerical approach. Using the scanned CAD model of the Atlantic white-sided dolphin (Lagenorhynchus acutus) and virtual skeleton-based surface reconstruction method, a three-dimensional high-fidelity computational model is obtained with time-varying kinematics. A sharp-interface immersed-boundary-method (IBM) based direct numerical simulation (DNS) solver is employed to calculate the corresponding thrust production, wake structure, and surface pressure at different swimming speeds. It is found that the fluke keeps its effective angle of attack at high values for about 60% of each stroke. The total pressure force coefficient along the x-axis converges as the speed increase. The flow and surface pressure analysis both show considerable differences between lower (2 m/s) and higher (5 m/s and 8 m/s) speeds. The results from this work help to bring new insight into understanding the force generation mechanisms of the highly efficient dolphin swimming and offer potential suggestions to the future designs of unmanned underwater vehicles.

Keywords: dolphin swimming, swimming speed, hydrodynamics, thrust, kinematics, vortex wake

NOMENCLATURE

A	peak-to-peak heaving amplitude of the fluke
C_P	hydrodynamic pressure coefficient
C_T	thrust force coefficient
f	fluke beat frequency
L	body length
Re	Reynolds number
S	wetted surface area of the body
St	Strouhal number
t	real time
T	fluke beat period
u_i	velocity components
U	swimming speed
U_{eff}	effective speed
V	flapping speed
α	effective angle of attack
θ	pitching angle of fluke
θ_0	pitching amplitude of fluke
ρ	density of the fluid
ν	kinematics viscosity

1. INTRODUCTION

Dolphins, known for their outstanding swimming performances, are of particular interest to the design of high-

---

[1] Contact author: haibo.dong@virginia.edu

performance underwater vehicles[1, 2]. Dolphins can achieve efficient swimming at various speeds[3, 4]. However, a clear understanding of their superior hydrodynamic performance, in terms of thrust production and the associated flow physics, especially at various speeds, remains elusive owing to technical difficulties of direct experimental measurements and limitations of computational tools.

Hydrodynamic force generation on the body surface and information about the flow field, such as pressure, velocity, and vorticity, are the key elements in understanding the flow mechanisms of dolphin swimming. However, it is extremely difficult to obtain the force or flow field information on dolphin swimming in the open ocean. Compared with experimental measurements, numerical simulations can obtain much more detailed force information relevant to the dolphin body and information of the flow field. Han et al.[5] studied the kinematics and hydrodynamics of a dolphin in forward swimming using direct numerical simulation and found that both the swimming kinematics and the resultant hydrodynamic force production and vortex wake formation are asymmetric between the downstroke and upstroke of the fluke. Tanaka et al. [6] measured the acceleration and deceleration of dolphin swimming and used Reynolds-Averaged Navier–Stokes (RANS) solver to calculate the hydrodynamic drag of a geometrically realistic but static dolphin model.

The previous numerical investigations were conducted either at only one swimming speed or using a static model. Therefore, in this work, the underlying mechanisms of dolphin swimming at three speeds, 2 m/s, 5 m/s, and 8 m/s, are explored using a combined experimental and numerical approach. Using the scanned CAD model of the Atlantic white-sided dolphin and virtual skeleton-based surface reconstruction method, a three-dimensional high-fidelity computational model is obtained with time-varying kinematics. A sharp-interface immersed-boundary-method (IBM) based direct numerical simulation (DNS) solver is employed to calculate the corresponding thrust production, wake structure, and surface pressure at different swimming speeds.

2. MATERIALS AND METHODS

2.1 Morphological and Kinematical Modeling of Dolphin Swimming

The body morphology of the dolphin (FIG. 1) is obtained from the 3D scanning of the adult female Atlantic white-sided dolphin (*Lagenorhynchus acutus*). The body length L is 2.2 m. The swimming kinematics are modeled at three different speeds, 2 m/s, 5 m/s, and 8 m/s, respectively. The corresponding fluke beat frequencies and pitching amplitude of the fluke are calculated based on empirical equations. For simplicity, the heaving amplitude of the fluke is kept constant. The swimming kinematics at 2 m/s during one fluke beat cycle is shown in FIG. 1. The pitching angle θ of the fluke is defined as the angle between the horizontal plane and the mid-chord of the fluke.

The kinematics information of the model at three speeds is listed in TAB. 1, where U is swimming speed, f is fluke beat frequency, A is the peak-to-peak heaving amplitude of fluke, and θ_0 is the pitching amplitude of fluke, respectively.

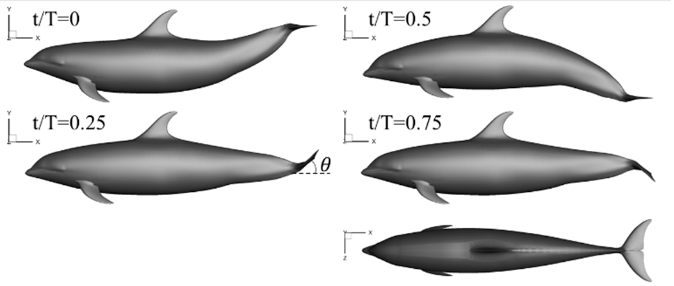

FIGURE 1: DOLPHIN MORPHOLOGY AND KINEMATICS AT 2 M/S. THE PITCHING ANGLE θ OF THE FLUKE IS DEFINED AS THE ANGLE BETWEEN THE HORIZONTAL PLANE AND THE MID-CHORD OF THE FLUKE.

TABLE 1: SUMMARY OF SWIMMING KINEMATICS

$\boldsymbol{U}$(m/s)	$\boldsymbol{f}$(Hz)	$\boldsymbol{A}$(m)	$\boldsymbol{\theta_0}$(deg.)
2	1.32	0.54	20
5	2.61	0.54	30
8	3.91	0.54	40

In flapping propulsion, owing to the unsteady flapping motion of the propulsor, the incoming flow experienced by the propulsor is no longer a constant horizontal flow, but a combined unsteady flow with changing velocity and direction. FIG. 1 shows the definition of the effective flow speed U_{eff}, and the effective angle of attack α. U is the swimming speed, and V is the instantaneous flapping speed of the fluke.

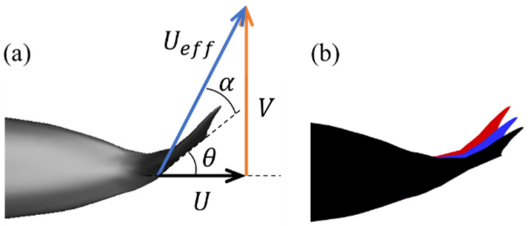

FIGURE 2: (A) DEFINITIONS OF EFFECTIVE ANGLE OF ATTACK α AND EFFECTIVE FLOW SPEED U_{eff}, AND (B) COMPARISON OF FLUKE PITCHING ANGLE AT MIDDLE DOWNSTROKE BETWEEN SWIMMING SPEEDS OF 2 M/S (RED), 5 M/S (BLUE), AND 8 M/S (BLACK), RESPECTIVELY.

Since U_{eff} and α are two critical factors that affect the hydrodynamic performance of the propulsor, the instantaneous normalized effective speed U_{eff}/U (FIG. 3) and effective angle of attack α (FIG. 4) are calculated compared between three speeds.

In FIG. 3, it is found that the U_{eff}/U reach their peak values at mid-strokes. The peak values of 2 m/s are around 2.2, which is considerably higher than those of the 5 m/s and 8 m/s which are between 1.7 and 1.9. In FIG. 4, it is found that as the swimming speed increase from 2 m/s to 8 m/s, the peak values of α decrease monotonically from around 42 degrees to 19 degrees. It is noteworthy that all α reach their peak values soon after the beginning of each stroke (around t/T=0.1, and t/T=0.6), and maintains their peak values till the very late of the stroke (around t/T=0.4, and t/T=0.9). This enables the fluke to keep its α at high values for about 60% of each stroke, extending the time for the fluke to generate thrust.

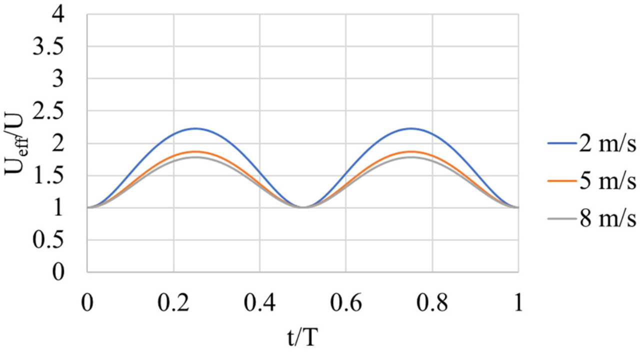

FIGURE 3: COMPARISON OF THE INSTANTANEOUS NORMALIZED EFFECTIVE SPEED (U_{eff}/U) OF FLUKE AT THREE SPEEDS

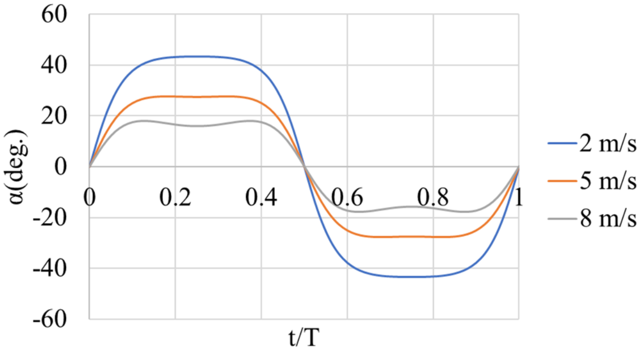

FIGURE 4: COMPARISON OF THE INSTANTANEOUS EFFECTIVE ANGLE OF ATTACK (α) OF FLUKE AT THREE SPEEDS

2.2 Numerical Method

The governing equations of the flow past the swimming dolphin solved in this paper are the incompressible Navier-Stokes equations, written in indicial form as,

$$\frac{\partial u_i}{\partial x_i} = 0; \; \frac{\partial u_i}{\partial t} + \frac{\partial u_i u_j}{\partial x_j} = -\frac{\partial p}{\partial x_i} + \frac{1}{Re}\frac{\partial^2 u_i}{\partial x_i \partial x_j} \qquad (1)$$

where u_i are the velocity components, p is the pressure, and Re is the Reynolds number.

The equations are solved using a Cartesian-grid-based sharp-interface immersed-boundary method[7], which has been successfully applied to simulate biological flapping propulsions including bird/insect flight[8-11] and fish swimming[12-16], and biomedical applications[17].

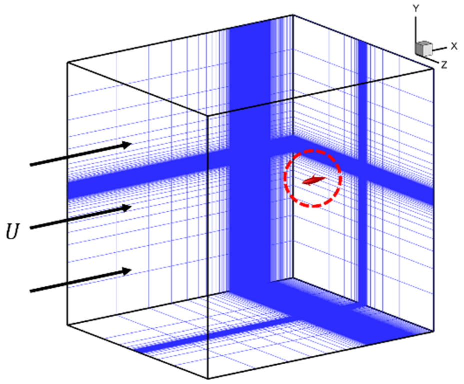

FIGURE 5: SCHEMATIC OF THE COMPUTATIONAL MESH USED IN THE PRESENT SIMULATION; THE DOLPHIN MODEL IS DENOTED BY THE DASHED CIRCLE.

A Cartesian computational grid with stretching grid configuration was employed in the simulations (FIG. 5). The computational domain size was $10L\times10L\times10L$ with total grid points around 9.6 million (385×193×129) and a minimum grid spacing at Δ_{min}=0.003L. The grid was designed to resolve the fluid field in the vicinity of the computational model and its wake with high resolution. The left-hand boundary was set as the velocity inlet with constant incoming flow speed U. A homogeneous Neumann boundary condition was used for the pressure at all boundaries. A No-slip boundary condition was applied at the model surface. The size of the computational domain was proven to be sufficiently large to obtain converged results by extensive simulation tests. In addition, a convergence study was performed to demonstrate the grid-independent results.

In this study, the key parameters associated with the flow simulation of dolphin swimming are the Reynolds number Re and the Strouhal number St defined as follows, respectively,

$$\mathrm{Re} = \frac{UL}{\nu}; \; \mathrm{St} = \frac{fA}{U} \qquad (2)$$

Where U is incoming flow pointing to x-positive, L is the body length of the dolphin, ν denotes the kinematic viscosity, f is the tail beat frequency, and A is the peak-to-peak amplitude of the fluke. The St for 2 m/s, 5 m/s, and 8 m/s are 0.35, 0.28, and 0.26, respectively. Limited by the computational resources, the Re of the simulation is reduced to 3000, 7500, and 12000, respectively.

3. RESULTS AND DISCUSSION

3.1 Hydrodynamic Performance

The hydrodynamic pressure force acting on the dolphin is computed by the direct integration of instantaneous pressure over the entire body surface. The total pressure force alone x-axis (F_x), is nondimensionalized as the coefficient $C_x|_{pressure}$ as,

$$C_x|_{pressure} = \frac{F_x}{\frac{1}{2}\rho U^2 S} \tag{3}$$

where, F_x points to x-positive, ρ is the fluid density, S denotes the wetted area of dolphin, and U is the swimming speed.

FIG. 6 compares the instantaneous $C_x|_{pressure}$ between three speeds. Positive $C_x|_{pressure}$ value means net drag, and a negative value means net thrust. It is found that, in general, the $C_x|_{pressure}$ of three speeds follow a similar trend. The x-force is lower at mid-strokes (t/T=3.1~3.3 and t/T=3.6~3.8), indicating larger thrust production of the fluke during mid-stroke when the effective angle of attack reaches its peak value. During the reversal of the fluke, the effective angle of attack is zero. Therefore, $C_x|_{pressure}$ is higher owing to the absence of thrust production from the fluke. It is also found that the $C_x|_{pressure}$ value converges as the speed increase. The $C_x|_{pressure}$ value is lower at lower swimming speed, indicating larger thrust production at the fluke than the drag production at the trunk of the dolphin.

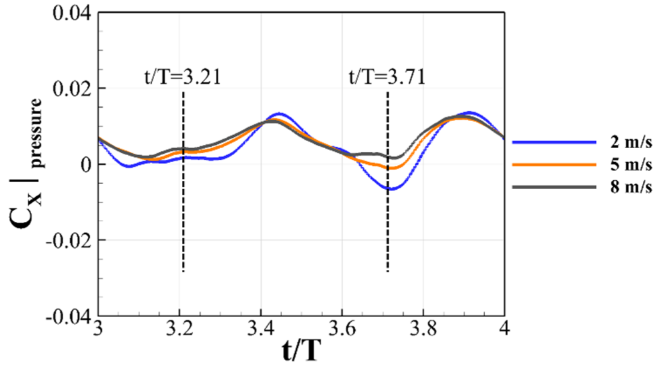

FIGURE 6: COMPARISON OF THE INSTANTANEOUS PRESSURE FORCE COEFFICIENT $C_x|_{pressure}$ OF THE DOLPHIN AT THREE SPEEDS

3.2 Wake Structure and Surface Pressure

FIG.7 shows the wake structure of the dolphin model swimming at 2 m/s. The λ-isosurface (FIG. 7a&b) and slice-cut of vorticity (FIG. 7c&d) are shown at two mid-strokes (t/T=3.21 (left) and t/T=3.71 (right)). It is found that a new vortex ring is generated during each stroke. The vortex rings form a von Kármán vortex street. A strong leading edge vortex (LEV) is formed at the fluke during mid-strokes, while shear layers are formed at the anterior body of the dolphin.

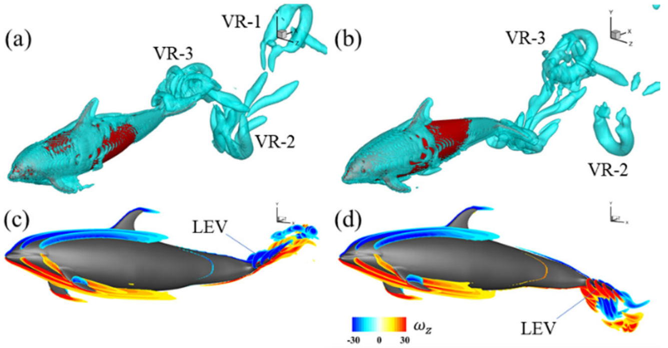

FIGURE 7: λ-ISOSURFACE (A AND B) AND VORTICITY (C AND D) AT t/T=3.21 (A AND C) AND t/T=3.71 (B AND D). THE λ-ISOSURFACE IS IDENTIFIED AT λ=2.5. THE VORTICITY ω_z IS NORMALIZED BY U/L.

FIG. 8 shows the instantaneous surface pressure of the dolphin model swimming at 2 m/s. The pressure contour is filled by C_p which is defined as $C_p = p/0.5\rho U^2$, where p is the dynamic pressure. The C_p contour at t/T=3.21 (FIG. 8a) and t/T=3.71 (FIG. 8b) are shown. It is found that owing to the formation of LEV, the suction side (blue) both has significantly low negative pressure at mid-stokes. However, the pressure side (red) at t/T=3.71 has a higher positive value than that at t/T=3.21, which explains the larger thrust generation at t/T=3.71.

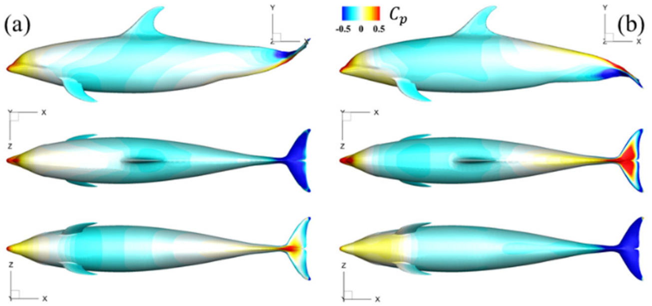

FIGURE 8: INSTANTANEOUS SURFACE PRESSURE C_p OF THE DOLPHIN MODEL SWIMMING AT 2 M/S WITH (A) AT t/T=3.21 AND (B) AT t/T=3.71

FIG. 9 shows the comparison of surface pressure on the fluke between 2 m/s, 5 m/s, and 8 m/s at t/T=3.71. It is found that they have similar negative pressure values at the suction side (blue). On the pressure side, the positive pressure of 2 m/s is significantly higher than those of the 5 m/s and 8 m/s, indicating a larger pressure difference between the two sides of the fluke and therefore more thrust generation. This explains the lower $C_x|_{pressure}$ in FIG. 6 which means higher thrust generation.

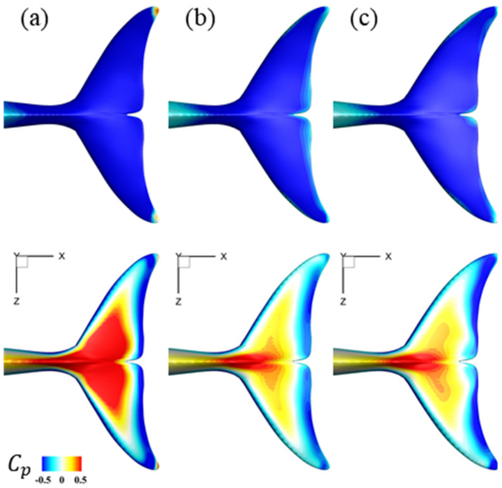

FIGURE 9: COMPARISON OF SURFACE PRESSURE C_p ON THE FLUKE BETWEEN 2 M/S (A), 5 M/S (B), AND 8 M/S (C) AT t/T=3.71

FIG 10 shows the comparison of vorticity around the fluke between three speeds. It is found that as the speed increases, both the LEV and trailing edge vortex (TEV) become more elongated. The TEV tip position also rolls up as the speed increases, which may explain the lower positive pressure at the suction side of speed 5 m/s and 8 m/s in FIG. 9.

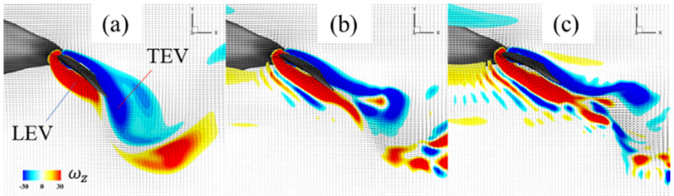

FIGURE 10: COMPARISON OF VORTICITY ω_z CONTOUR ON A SLICE-CUT THROUGH THE FLUKE BETWEEN 2 M/S (A), 5 M/S (B), AND 8 M/S (C) AT t/T=3.71

4. CONCLUSION

It is found that the fluke keeps its effective angle of attack at high values for about 60% of each stroke. The total pressure force coefficient along the x-axis converges as the speed increase. The LEV of the lower speed (2 m/s) is more coherent and less elongated than those of the higher speed (5 m/s and 8 m/s), resulting in larger positive pressure on the pressure side and the consequently larger pressure difference between the pressure side and the suction side, which produces more thrust.

ACKNOWLEDGEMENTS

This research is supported by ONR MURI grant no. N00014-14-1-0533, NSF CNS grant no. CPS-1931929, ASME FED GSS, and School of Engineering and Applied Science Distinguished Fellowship of the University of Virginia

REFERENCES

[1] Fish, F. E., 2020, "Advantages of aquatic animals as models for bio-inspired drones over present AUV technology," Bioinspiration & Biomimetics, 15(2), p. 025001.

[2] Roper, D. T., Sharma, S., Sutton, R., and Culverhouse, P., 2011, "A review of developments towards biologically inspired propulsion systems for autonomous underwater vehicles," Proceedings of the Institution of Mechanical Engineers, Part M: Journal of Engineering for the Maritime Environment, 225(2), pp. 77-96.

[3] Fish, F. E., and Rohr, J., 1999, "Review of dolphin hydrodynamics and swimming performance," Space and Naval Warfare Systems Command San Diego CA, pp. No. SPAWAR/CA-TR-1801.

[4] Fish, F. E., 2006, "The myth and reality of Gray's paradox: implication of dolphin drag reduction for technology," Bioinspiration & Biomimetics, 1(2), pp. R17-R25.

[5] Han, P., Wang, J., Fish, F. E., and Dong, H., 2020, "Kinematics and Hydrodynamics of a Dolphin in Forward Swimming," AIAA AVIATION 2020 FORUM, American Institute of Aeronautics and Astronautics, pp. 2020-3015.

[6] Tanaka, H., Li, G., Uchida, Y., Nakamura, M., Ikeda, T., and Liu, H., 2019, "Measurement of time-varying kinematics of a dolphin in burst accelerating swimming," PLOS ONE, 14(1), p. e0210860.

[7] Mittal, R., Dong, H., Bozkurttas, M., Najjar, F. M., Vargas, A., and von Loebbecke, A., 2008, "A versatile sharp interface immersed boundary method for incompressible flows with complex boundaries," Journal of Computational Physics, 227(10), pp. 4825-4852.

[8] Wang, J., Ren, Y., Li, C., and Dong, H., 2019, "Computational investigation of wing-body interaction and its lift enhancement effect in hummingbird forward flight," Bioinspiration & Biomimetics, 14(4), p. 046010.

[9] Liu, G., Dong, H., and Li, C., 2016, "Vortex dynamics and new lift enhancement mechanism of wing–body interaction in insect forward flight," Journal of Fluid Mechanics, 795, pp. 634-651.

[10] Bode-Oke, A. T., Zeyghami, S., and Dong, H., 2018, "Flying in reverse: kinematics and aerodynamics of a dragonfly in backward free flight," Journal of The Royal Society Interface, 15(143), p. 20180102.

[11] Pan, Y., Wang, J., and Dong, H., 2019, "Study on the passive pitching mechanism of different forms of flapping motion in turning flight," AIAA Aviation 2019 Forum, American Institute of Aeronautics and Astronautics, pp. 2019-3435.

[12] Liu, G., Ren, Y., Dong, H., Akanyeti, O., Liao, J. C., and Lauder, G. V., 2017, "Computational analysis of vortex dynamics and performance enhancement due to body-fin and fin-fin interactions in fish-like locomotion," Journal of Fluid Mechanics, 829, pp. 65-88.

[13] Wang, J., Wainwright, D. K., Lindengren, R. E., Lauder, G. V., and Dong, H., 2020, "Tuna locomotion: a computational hydrodynamic analysis of finlet function," Journal of The Royal Society Interface, 17(165), p. 20190590.

[14] Pan, Y., and Dong, H., 2020, "Computational analysis of hydrodynamic interactions in a high-density fish school," Physics of Fluids, 32(12), p. 121901.

[15] Narasimhan, M., Dong, H., Mittal, R., and Singh, S. N., 2005, "Optimal Yaw Regulation and Trajectory Control of Biorobotic AUV Using Mechanical Fins Based on CFD Parametrization," Journal of Fluids Engineering, 128(4), pp. 687-698.

[16] Pan, Y., Han, P., Huang, J., and Dong, H., 2020, "Effect of Formation Pattern on Schooling Energetics in Fish-Like Swimming," ASME 2020 Fluids Engineering Division Summer Meeting collocated with the ASME 2020 Heat Transfer Summer Conference and the ASME 2020 18th International Conference on Nanochannels, Microchannels, and Minichannels, p. V003T005A046.

[17] Wang, J., Xi, J., Han, P., Wongwiset, N., Pontius, J., and Dong, H., 2019, "Computational analysis of a flapping uvula on aerodynamics and pharyngeal wall collapsibility in sleep apnea," Journal of Biomechanics, 94, pp. 88-98.